

## ELLIPSOIDAL COLLAPSE AND PREVIRIALIZATION

A. DEL POPOLO,<sup>1,2</sup> E. N. ERCAN,<sup>3</sup> AND Z. XIA<sup>4</sup>

Received 2001 February 25; accepted 2001 April 9

### ABSTRACT

We study the nonlinear evolution of a dust ellipsoid embedded in a flat Friedmann background universe, in order to determine the evolution of the density of the ellipsoid as the perturbation associated with it detaches from the general expansion and begins to collapse. We show that while the growth rate of the density contrast of a mass element is enhanced by shear, in agreement with Hoffman's 1986 result, the angular momentum acquired by the ellipsoid has the right magnitude to counterbalance the effect of the shear. This result confirms the previrialization conjecture by showing that initial asphericities and tidal interactions begin to slow the collapse after the system has broken away from the general expansion.

*Key words:* cosmology: theory — galaxies: formation

### 1. INTRODUCTION

While cosmologists generally believe that structures in the universe grew via gravitational instability from smaller inhomogeneities present at the epoch of decoupling, there is disagreement on several details of the model. One of these is the role of asphericity in the collapse of perturbations and structure formation.

According to the previrialization conjecture (Peebles & Groth 1976; Davis & Peebles 1977; Peebles 1990), initial asphericities and tidal interactions between neighboring density fluctuations induce significant nonradial motions that oppose collapse. This means that virialized clumps form later, with respect to the predictions of linear perturbation theory or the spherical collapse model, and that the initial density contrast needed to obtain a given final density contrast must be larger than that for an isolated spherical fluctuation. This kind of conclusion has been supported by Barrow & Silk (1981), Szalay & Silk (1983), Villumsen & Davis (1986), Bond & Myers (1996a, 1996b), and Łokas et al. (1996).

In particular, Barrow & Silk (1981) and Szalay & Silk (1983) pointed out that nonradial motions would slow the rate of growth of the density contrast, by lowering the peculiar velocity, and suppress collapse once a system detached from the general expansion. Villumsen & Davis (1986) gave examples of the growth of nonradial motions in  $N$ -body simulations. Arguments based on a numerical least-action method led Peebles (1990) to the conclusion that irregularities in the mass distribution, together with external tides, induce nonradial motions that slow down the collapse. Łokas et al. (1996) used  $N$ -body simulations and a weakly nonlinear perturbative approach to study previrialization. They concluded that when the slope of the initial power spectrum  $n > -1$ , nonlinear tidal interactions slow down the growth of density fluctuations, and the magnitude of the effect increases when  $n$  is increased.

Opposite conclusions were obtained by Hoffman (1986b, 1989), Evrard & Crone (1992), Bertschinger & Jain (1994), and Monaco (1995). In particular, Hoffman (1986b, 1989), using the quasi-linear approximation (Zeldovich 1970; Zeldovich & Novikov 1983), showed that shear affects the dynamics of collapsing objects and leads to infall velocities that are higher than in the shear-free case. Bertschinger & Jain (1994) put this result into theorem form, according to which spherical perturbations are the slowest in collapsing. The  $N$ -body simulations by Evrard & Crone (1992) did not reproduce the previrialization effect, but the reason is due to their assumption of an  $n = -1$  spectrum, different from the  $n = 0$  one used by Peebles (1990) that reproduced the effect. If  $n < -1$ , the peculiar gravitational acceleration,  $g \propto R^{-(n+1)/2}$ , diverges at large  $R$  and the gravitational acceleration moves the fluid more or less uniformly, generating bulk flows rather than shearing motions. Therefore, the collapse will be similar to that of an isolated spherical clump. If  $n > -1$ , the dominant sources of acceleration are local, small-scale inhomogeneities, and tidal effects will tend to generate nonradial motions and resist gravitational collapse.

In a more recent paper, Audit, Teyssier, & Alimi (1997) proposed some analytic prescriptions for computing the collapse time along the second and third principal axes of an ellipsoid, by means of the “fuzzy” threshold approach. They point out that the formation of real virialized clumps must correspond to third-axis collapse and that collapse along this axis is slowed down by the effect of shear rather than being accelerated by it, in contrast to its effect on first-axis collapse. They conclude that spherical collapse is the fastest, in disagreement with Bertschinger & Jain's theorem. This result is in agreement with Peebles (1990).

In this paper, we address this controversy by following the evolution of a dust ellipsoid in an expanding universe. We shall use a model by Nariai & Fujimoto (1972) that makes it possible to study separately the effect of the shear,  $\Sigma$ , and that of angular momentum,  $L$ , on the protostructure's evolution.

The paper is organized as follows: In § 2, we describe the model used; in § 3, we calculate the angular momentum of the ellipsoid at an intermediate time between the turnaround of the first and third axes; and in § 4, we describe the parameters and initial conditions used. Section 5 is devoted to the discussion of results, and § 6 to conclusions.

<sup>1</sup> Dipartimento di Matematica, Università Statale di Bergamo, Piazza Rosate 2, I-24129 Bergamo, Italy.

<sup>2</sup> Also Feza Gürsey Enstitüsü, P.K. 6, 81220 Çengelköy, İstanbul, Turkey; and Boğaziçi Üniversitesi, 80815 Bebek, İstanbul, Turkey.

<sup>3</sup> Fizik Bölümü, Boğaziçi Üniversitesi, 80815 Bebek, İstanbul, Turkey.

<sup>4</sup> Center for Optimization Research and Applications, Department of Applied Mathematics, Dalian University of Technology, 116024 Dalian, China.

## 2. ELLIPSOID MODEL FOR THE COLLAPSE

In order to determine the evolution of the density in an ellipsoid of ideal fluid at zero pressure, we follow Nariai & Fujimoto (1972) and Barrow & Silk (1981). In what follows, we shall study the evolution of the density,  $\rho$ , of an ellipsoid embedded in a pressureless background cosmology with zero curvature characterized by a background density  $\rho_b$  and expansion parameter  $a(t)$ :

$$\rho_b = \frac{1}{6\pi G t^2}, \quad a \propto t^{2/3}. \quad (1)$$

As shown by Nariai & Fujimoto (1972), performing two transformations of coordinates, from the comoving frame  $\{\hat{x}^\mu\}$  to the inertial frame  $x^\mu = (t, x^i)$  with

$$x^i = a(t)\hat{x}^i \quad (2)$$

and then to a noninertial system of reference,  $\{(x')^\mu\}$ , rotating with angular velocity  $\Omega_i$  with respect to the inertial frame  $\{x^i\}$ , the Newtonian hydrodynamic equations of continuity and motion and Poisson's equation are

$$\frac{d\rho}{dt} + \frac{\partial V'_i}{\partial x'_i} \rho = 0, \quad (3)$$

$$\frac{dV'_i}{dt} + 2\epsilon_{ijk}\Omega_j V'_k = \frac{1}{\rho} \frac{\partial p}{\partial x'_i} - \frac{\partial \phi}{\partial x'_i} - \left[ \left( \frac{4\pi G}{3} \rho_b - \Omega^2 \right) \delta_{ij} + \Omega_i \Omega_j - \epsilon_{ijk} \frac{d\Omega_k}{dt} \right] x'_j, \quad (4)$$

$$\nabla^2 \phi = 4\pi G(\rho - \rho_b), \quad (5)$$

where  $\rho$  and  $p$  are the density and pressure perturbations and (hereafter denoting  $x'_i$  and  $V'_i$  by  $x_i$  and  $V_i$ , respectively)

$$\frac{d}{dt} \equiv \partial_t + V_i \frac{\partial}{\partial x_i}. \quad (6)$$

Considering a rotating ellipsoid of uniform density,  $\rho = \rho(t)$ , the velocity field is given by

$$V_i = \alpha_{ij} x_j \quad (7)$$

with

$$\alpha_{ij} = \left[ \frac{1}{3} \left( \frac{\dot{\alpha}_1}{\alpha_1} + \frac{\dot{\alpha}_2}{\alpha_2} + \frac{\dot{\alpha}_3}{\alpha_3} \right) \delta_{ij} + \Sigma_{ij} + \epsilon_{ijk} \omega_k \right], \quad (8)$$

where the shear tensor,  $\Sigma_{ij}$ , and the vorticity vector,  $\omega_k$ , are given by

$$\Sigma_{ij} \equiv \frac{1}{2}(\alpha_{ij} + \alpha_{ji}) - \frac{1}{3}\alpha_{kk} \delta_{ij}, \quad (9)$$

$$\omega_i \equiv \epsilon_{ijk} \alpha_{jk}. \quad (10)$$

The term  $\alpha_i$  represents the  $i$ th principal semiaxis of the ellipsoid. Assuming that the rotation velocity possesses only an  $x_3$ -component and that the initial vorticity (note that here the term "initial vorticity" is not to be interpreted as primordial vorticity, which is zero before orbit crossing, but as the vorticity acquired after shell crossing) has no components in the directions of  $x_1$  and  $x_2$ , then the equations of motion for the principal axes of the ellipsoid and that for

the evolution of the density are

$$\ddot{\alpha}_1 = -\frac{4\pi G}{3} \rho_b \left( 1 - \frac{3}{2} \alpha_1 \alpha_2 \alpha_3 U_1 \right) \alpha_1 - \frac{3}{2} GM U_1 \alpha_1 + \frac{8L^2}{(\alpha_1 + \alpha_2)^3}, \quad (11)$$

$$\ddot{\alpha}_2 = -\frac{4\pi G}{3} \rho_b \left( 1 - \frac{3}{2} \alpha_1 \alpha_2 \alpha_3 U_2 \right) \alpha_2 - \frac{3}{2} GM U_2 \alpha_2 + \frac{8L^2}{(\alpha_1 + \alpha_2)^3}, \quad (12)$$

$$\ddot{\alpha}_3 = -\frac{4\pi G}{3} \rho_b \left( 1 - \frac{3}{2} \alpha_1 \alpha_2 \alpha_3 U_3 \right) \alpha_3 - \frac{3}{2} GM U_3 \alpha_3, \quad (13)$$

$$\frac{\ddot{\rho}}{\rho} - \frac{4}{3} \left( \frac{\dot{\rho}}{\rho} \right)^2 - 4\pi G \rho - \Sigma^2 + \frac{8L^2}{\alpha_1 \alpha_2 (\alpha_1 + \alpha_2)^2} = 0 \quad (14)$$

(Nariai & Fujimoto 1972; Barrow & Silk 1981), where  $L$  is the angular momentum of the ellipsoid and

$$U_i = \int_0^\infty \frac{dx}{(\alpha_i^2 + x)\psi^{1/2}(x)}, \quad (15)$$

$$\psi(x) = \prod_{i=1}^3 (\alpha_i^2 + x), \quad (16)$$

$$M = \frac{4\pi}{3} \rho \alpha_1 \alpha_2 \alpha_3 = \text{const}, \quad (17)$$

$$\Sigma^2 = \sum_{i=1}^3 \Sigma_i^2 = \Sigma_1^2 + \Sigma_2^2 + \Sigma_3^2 \quad (18)$$

(see eq. [3.22] of Nariai & Fujimoto 1972). Equation (14), even if not strictly necessary to describe the evolution of the ellipsoid, is very useful because it allows us to qualitatively understand how the gravitational instability process is modified by the rotation and shear anisotropy. If  $\Sigma = L = 0$ , we are brought back to the spherically symmetric case of no rotation. In this event, the density reaches a maximum value of  $9\pi^2/16\rho_b$ , and afterward the system recollapses. The shear,  $\Sigma^2$ , acts in the same sense as gravity, making collapse easier, while the angular momentum  $L$  acts in the sense opposite to self-gravity,  $G\rho$ , making it easier to resist gravitational collapse. Obviously, equation (14) could be also used to obtain the evolution of the density after calculating  $\Sigma^2$  and  $L^2$ . As shown by Nariai & Fujimoto,  $\Sigma^2$  is given by equation (18), and  $\Sigma_i$  can be obtained by means of equation (9) and equation (3.4) of Nariai & Fujimoto (1972) as follows:

$$\Sigma_i \equiv \Sigma_{ii} = \frac{1}{3} \left( 2 \frac{\dot{\alpha}_i}{\alpha_i} - \frac{\dot{\alpha}_j}{\alpha_j} - \frac{\dot{\alpha}_k}{\alpha_k} \right), \quad (19)$$

This last result shows even more clearly that equations (11)–(13) form a closed system giving the evolution of the ellipsoid and the shear.

The evolution of the density can then be obtained (once the angular momentum is known) in two ways:

1. By integrating equations (11)–(13) to determine the evolution of the semiaxes, in which case  $\Sigma^2$  can be calcu-

lated through equations (19) and (18) and the density evolution finally obtained by integrating equation (14);

2. By integrating equations (11)–(13) to determine the evolution of the semiaxes and then using equation (17).

It is useful to note that while procedure 2 is simpler than 1 if  $\Sigma \neq 0$ , when  $L = \Sigma = 0$  it is simpler to use procedure 1 because, in this case, we know a priori that  $\Sigma = 0$ , and consequently we have only to perform the integration of equation (14). If, otherwise, we wanted to use procedure 2, we should integrate equations (11)–(13) and also impose the condition that  $\Sigma^2 = 0$  using equation (19), with a consequent complication of the calculations. In any case, in this paper we performed the calculations following both procedures, in order to check the consistency of the results.

A fundamental point to make is the following: the Nariai & Fujimoto (1972) equations give a description of the evolution and collapse of an ellipsoid only if the ellipsoid has somehow acquired angular momentum. For the reasons that follow, we use this model to study the evolution of the ellipsoid from the epoch of turnaround of the first axis onward.

An ellipsoid can have angular momentum for two different reasons:

1. The axes of the ellipsoid and that of the shear of the velocity field have an appropriate misalignment, or in other words, the principal axes of the inertia tensor are not aligned with the principal axes of the deformation tensor (see Catelan & Theuns 1996a, 1996b). In this case, the ellipsoid can have angular momentum even if the vorticity is zero. We are not interested in this particular case.

2. The system has a nonzero vorticity. Unfortunately, we know that according to Kelvin's theorem, if the initial velocity field is irrotational, i.e., curl-free, then it should remain irrotational in the nonlinear regime. However, since the collapse of a protostructure is a violent phenomenon, the conditions of Kelvin's circulation theorem should be violated (Chernin 1970). Then there are two possibilities for vorticity generation (see Sasaki & Kasai 1998):

a) Acquisition of vorticity by the formation of shock fronts in the protostructure (pancake), corresponding to shell crossing (Doroshkevich 1970). Analytical studies by Pichon & Bernardeau (1999) have also shown that vorticity generation becomes significant at scales of 3–4  $h^{-1}$  Mpc and increases with decreasing scale.

b) Acquisition of angular momentum by means of tidal torques (Hoyle 1951; Peebles 1969; Hoffman 1986a; Ryden & Gunn 1987). Current analytical descriptions of vorticity and spin growth by tidal torques turn out to depend on a free parameter, i.e., the time when the tidal torques cut off. This parameter has been related to either the beginning of decoupling from the Hubble flow ( $\delta \simeq 1$ ) or the turnaround epoch (time when expansion halts) (for the spherical collapse model; Andriani & Caimmi 1994). Numerical simulations (Barnes & Efstathiou 1987) have shown that after decoupling from the Hubble flow, there is no substantial increment in angular momentum.

Summarizing, we know (and assume) that from the linear phase to shell crossing the vorticity is zero; the ellipsoid has no rotation. The perturbation is subject to the gravitational field of matter inside the ellipsoid, which tends to make it collapse into a pancake, and to the tidal field of the matter outside, which cancels the effects of the interior gravita-

tional field. As a result, the ellipsoid expands with the rest of the universe and preserves its shape until it enters the nonlinear phase (Barrow & Silk 1981; White & Silk 1979). When it reaches a density contrast  $\delta \simeq 1$ , it detaches from Hubble expansion and the distribution of matter of the ellipsoid tends to develop nonradial motions (Peebles 1980), even if the axes of the ellipsoid and the shear of the velocity field do not have an appropriate misalignment.

To take account of the rotation acquired, we identify the final angular momentum of the ellipsoid with that acquired at the maximum of the object's expansion (Peebles 1969; Catelan & Theuns 1996a, 1996b). This assumption is justified by the fact that after the maximum expansion time the angular momentum stops growing, becoming less sensitive to tidal couplings (Peebles 1969; Barnes & Efstathiou 1987).

In other words, we assume that the total angular momentum is acquired before the ellipsoid's collapse, since the tidal torques are much less effective afterward (Peebles 1969; Catelan & Theuns 1996a, 1996b). While for a spherical perturbation this time is well defined (it is the turnaround epoch), for an aspherical perturbation this epoch is not well defined, and the system should be followed until the long axis turns around (Eisenstein & Loeb 1995), since the acquisition of angular momentum is important until the collapse of this axis. To simplify things, we choose a mean value for the time,  $t_M$ , between the turnaround of the shortest axis and that of the longest (see Hoffman 1986a)

### 3. ANGULAR MOMENTUM AT $t_M$

As previously remarked, if we want equations (11)–(13) to constitute a closed system in order to determine the ellipsoid's evolution, we need the angular momentum  $L$ . As stressed above, we need only the value of the angular momentum of the virialized structure, which can be well approximated (see the above discussion) by its value at the time  $t_M$ .

The effect of tidal torques on structures' evolution has been studied in several papers, especially in connection with the origin of galaxies' rotation. The explanation of how galaxies gain spin through tidal torques was pioneered by Hoyle (1951) in the context of a collapsing protogalaxy. Peebles (1969) considered the process in the context of an expanding world model, showing that the angular momentum gained by the matter in a random comoving *Eulerian* sphere grows to second order in proportion to  $t^{5/3}$  (in an Einstein–de Sitter universe), since the protogalaxy still represented a small perturbation, while in the nonlinear stage the growth rate of an oblate homogeneous spheroid decreases with time as  $t^{-1}$ .

White (1984) considered an analysis by Doroshkevich (1970) that showed that the angular momentum of galaxies grows to first order in proportion to  $t$  and that Peebles's result is a consequence of the spherical symmetry imposed on the model. White showed that the angular momentum of a Lagrangian sphere does not grow either in the first or in the second order, while the angular momentum of a non-spherical volume grows to first order in agreement with Doroshkevich's result.

Another way to study the acquisition of angular momentum by a protostructure is that followed by Ryden (1988, hereafter R88) and by Eisenstein & Loeb (1995). Following Eisenstein & Loeb, we separate the universe into two disjoint parts: the collapsing region, characterized by having high density, and the rest of the universe. The boundary

between these two regions is taken to be a sphere centered on the origin. As usual, in the following we denote the density as a function of space by  $\rho(x)$ ,  $x$  being the position vector, and  $\delta(x) = [\rho(x) - \rho_b]/\rho_b$ . The gravitational force exerted on the spherical central region by the external universe can be calculated by expanding the potential,  $\Phi(x)$ , in spherical harmonics. Assuming that the sphere has radius  $R$ , we have

$$\Phi(x) = \sum_{l=0}^{\infty} \frac{4\pi}{2l+1} \sum_{m=-l}^l a_{lm}(x) Y_{lm}(\theta, \phi) x^l, \quad (20)$$

where  $Y_{lm}$  are spherical harmonics and the tidal moments,  $a_{lm}$ , are given by

$$a_{lm}(x) = \rho_b \int_R^{\infty} Y_{lm}(\theta, \phi) \rho(s) s^{-l-1} d^3s. \quad (21)$$

In this approach, the protostructure is divided into a series of mass shells and the torque on each mass shell is computed separately. The density profile of each protostructure is approximated by the superposition of a spherical profile,  $\delta(r)$ , and the same Gaussian density field that is found far from the peak,  $\epsilon(r)$ , which provides the quadrupole moment of the protostructure. To first order, the asphericity about a given peak can be represented writing the initial density in the form

$$\rho(r) = \rho_b [1 + \delta(r)] [1 + \epsilon(r)] \quad (22)$$

(Ryden & Gunn 1987; R88; Peebles 1980, eq. [18.5]), where  $\epsilon(r)$  satisfies the equations

$$\langle |\epsilon_k|^2 \rangle = P(k), \quad (23)$$

$P(k)$  being the power spectrum, and

$$\langle \epsilon(r) \rangle = 0, \quad \langle \epsilon(r)^2 \rangle = \xi(0) \quad (24)$$

(Ryden & Gunn 1987; Peebles 1980), where angle brackets indicate a mean value of the physical quantity considered and  $\xi$  is the two-point correlation function. (Note that the previous equations are obtained in the lowest order approximation. The limits of the same are described in Ryden & Gunn 1987.) The torque on a thin spherical shell of internal radius  $x$  is given by

$$\tau(x) = -\frac{GM_{\text{sh}}}{4\pi} \int \epsilon(x) x \times \nabla \Phi(x) d\Omega, \quad (25)$$

where  $M_{\text{sh}} = 4\pi\rho_b[1 + \delta(x)]x^2\delta x$ . Before going on, recall that we are interested in the acquisition of angular momentum from the inner region, and for this purpose we take account only of the  $l=2$  (quadrupole) term. In fact, the  $l=0$  term produces no force, while the dipole ( $l=1$ ) cannot change the shape or induce any rotation of the inner region. As shown by Eisenstein & Loeb (1995), in the standard cold dark matter scenario the dipole is generated at large scales, so the object we are studying and its neighborhood move as a bulk flow, with the consequence that the angular distribution of matter will be very small, and then the dipole terms can be ignored. Because of the isotropy of the random field,  $\epsilon(x)$ , equation (25) can be written

$$\begin{aligned} \langle |\tau|^2 \rangle &= \sqrt{30} \frac{4\pi G}{5} \\ &\times [\langle a_{2m}(x)^2 \rangle \langle q_{2m}(x)^2 \rangle - \langle a_{2m}(x) q_{2m}^*(x) \rangle^2]^{1/2}. \quad (26) \end{aligned}$$

As stressed in the next section, following Eisenstein & Loeb (1995), the integration of the equations of motion shall be ended at some time before the inner external tidal shell (i.e., the innermost shell of the part of the universe outside the sphere containing the ellipsoid) collapses. Then the inner region behaves as a density peak. This last point is an important one in the development of the present paper.

An important question to ask before continuing regards the role of the triaxiality of the ellipsoid (density peak) in generating a quadrupole moment. Equation (26) takes into account the quadrupole moment that comes from the secondary perturbation near the peak. The density distribution around the inner region is characterized by a mean spherical distribution,  $\delta$ , and a random isotropic field (see eq. [22]). In reality, the central region is a triaxial ellipsoid. It is thus important to evaluate the contribution to the quadrupole moment due to the triaxiality. Remembering that the quadrupole moments are given by

$$\begin{aligned} q_{2m} &= \int_{|r|<R} Y_{2m}^*(\theta, \phi) s^2 \rho(s) d^3s \\ &= \frac{x^2 M_{\text{sh}}}{4\pi} \int Y_{2m}^*(\theta, \phi) \epsilon(x) d\Omega, \quad (27) \end{aligned}$$

we approximate the density profile as

$$\delta(x) = \langle \delta(x) \rangle_{\text{sph}} + v f(x) A(e, p), \quad (28)$$

$\langle \delta(x) \rangle_{\text{sph}}$  being the mean spherical profile,  $v = \delta/\sigma$  the peak height, and  $\sigma$  the rms value of  $\delta$ . The function  $A(e, p)$  of the triaxiality parameters,  $e$  and  $p$ , is given by

$$\begin{aligned} A(e, p) &= 3e(1 - \sin^2 \theta - \sin^2 \theta \sin^2 \phi) \\ &+ p(1 - 3 \sin^2 \theta \cos^2 \phi), \quad (29) \end{aligned}$$

while the function  $f(x)$  is given by

$$f(x) = \frac{5}{2\sigma} R_*^2 \left( \frac{1}{x} \frac{d\xi}{dx} - \frac{1}{3} \nabla^2 \xi \right) \quad (30)$$

(R88), where  $\xi$ ,  $\sigma$ , and  $R_*$  are respectively the two-point correlation function, the mass variance, and a parameter connected to the spectral moments (see eq. [4.6d] of Bardeen et al. 1986, hereafter BBKS). Substituting equations (28) and (29) into equation (27), it is easy to show that the sum of the mean quadrupole moments due to triaxiality is

$$\begin{aligned} \frac{1}{M_{\text{sh}}} \sum_{m=-2}^2 \langle q_{2m}(x) \rangle &= vx^2 f(x) \\ &\times \left[ \frac{1}{2\pi} \sqrt{\frac{6\pi}{5}} (e - p) + \frac{1}{4\pi} \sqrt{\frac{4\pi}{5}} (3e + p) \right], \quad (31) \end{aligned}$$

which must be compared with that produced by the secondary perturbations,  $\epsilon$ :

$$\langle q_{2m}(x)^2 \rangle = \frac{x^4}{(2\pi)^3} M_{\text{sh}}^2 \int k^2 P(k) j_2(kx)^2 dk, \quad (32)$$

where  $j_2$  is the Bessel function of order 2. The values of  $e$  and  $p$  can be obtained from the distribution of ellipticity and prolateness (BBKS, eq. [7.6] and Fig. 7) or, for  $v > 2$ ,

from

$$e = \frac{1}{\sqrt{5x[1 + 6/(5x^2)]^{1/2}}}, \quad p = \frac{6}{5x^4[1 + 6/(5x^2)]^2} \quad (33)$$

(BBKS, eq. [7.7]), where  $x$  is also given in BBKS (eq. [6.13]). In the case of a peak with  $\nu = 3$ , we have  $e \simeq 0.15$  and  $p \simeq 0.014$ , while for peaks having  $\nu = 2$  and  $\nu = 1$ , the values are respectively given by  $e \simeq 0.2$ ,  $p \simeq 0.03$  and  $e \simeq 0.25$ ,  $p \simeq 0.04$ .

As shown in Figure 1, for a  $3\sigma$  profile, the quadrupole moment due to triaxiality is less important than that produced by the random perturbations  $\epsilon$  in all of the proto-structure except the central regions, where the quadrupole moment due to triaxiality is comparable in magnitude to that due to secondary perturbations. In other words, the triaxiality has a significant effect only in the very central regions, which contain no more than a few percent of the total mass and where the acquisition of angular momentum is negligible. It follows that the triaxiality can be ignored while computing both expansion and spin growth (R88). Moreover, as observed by Eisenstein & Loeb (1995), the ellipsoid model does better in describing low-shear regions (having higher values of  $\nu$ ), for which collapse is more spherical and the effects of triaxiality are less evident. Just these peaks, having at least  $\nu > 2$ , will be studied in this paper. In any case, even if the triaxiality is not negligible it should contribute incrementally to the acquisition of angular momentum (Eisenstein & Loeb 1995), finally yielding a larger effect on the density evolution (i.e., a larger reduction of the growth rate of the density).

In order to find the total angular momentum imparted to a mass shell by tidal torques, it is necessary to know the time dependence of the torque. This can be accomplished by connecting the  $q_{2m}$  and  $a_{2m}$  to the parameters of the spher-

ical collapse model (Eisenstein & Loeb 1995, eq. [32]; R88, eqs. [32] and [34]). Following R88, we have

$$q_{2m}(\theta) = \frac{1}{4} q_{2m,0} \bar{\delta}_0^{-3} \frac{(1 - \cos \theta)^2 f_2(\theta)}{f_1(\theta) - (\delta_0/\bar{\delta}_0) f_2(\theta)}, \quad (34)$$

$$a_{2m}(\theta) = a_{2m,0} (4/3)^{4/3} \bar{\delta}_0 (\theta - \sin \theta)^{-4/3}. \quad (35)$$

The collapse parameter  $\theta$  is given by

$$t(\theta) = \frac{3}{4} t_0 \bar{\delta}_0^{-3/2} (\theta - \sin \theta). \quad (36)$$

Equations (34) and (35), by means of equation (26), give us the tidal torque:

$$\tau(\theta) = \tau_0 \frac{1}{3} \left(\frac{4}{3}\right)^{1/3} \bar{\delta}_0^{-1} \frac{(1 - \cos \theta)^2}{(\theta - \sin \theta)^{4/3}} \frac{f_2(\theta)}{f_1(\theta) - (\delta_0/\bar{\delta}_0) f_2(\theta)}, \quad (37)$$

where  $f_1(\theta)$  and  $f_2(\theta)$  are given in R88 (eq. [31]) and  $\tau_0$  and  $\delta_0 = (\rho - \rho_b)/\rho_b$  are respectively the torque and the mean fractional density excess inside the shell as measured at the current epoch,  $t_0$ . The angular momentum acquired during expansion can then be obtained by integrating the torque over time:

$$L = \int \tau(\theta) \frac{dt}{d\theta} d\theta. \quad (38)$$

As remarked in the previous section, the angular momentum obtained from equation (38) is evaluated at the time  $t_M$ . Then the calculation of the angular momentum can be accomplished by means of equation (38), once we have made a choice for the power spectrum. With the power spectrum and the parameters given in the next section and for a  $\nu = 2$  peak, the model gives a value of  $2.5 \times 10^{74} \text{ g cm}^2 \text{ s}^{-1}$ .

Since the calculation of the angular momentum is fundamental for the evolution of the ellipsoid, it is worthwhile to comment on the validity of the calculation and the result.

To start with, we want to recall that, independently of the calculation followed in order to determine the angular momentum, we need only its final value. Then it becomes important to compare the result obtained with our approach with those obtained following different approaches. An interesting comparison can be made with the result of Catelan & Theuns (1996a), who calculated the angular momentum at maximum expansion time (see their eqs. [31]–[32]) and compared it with previous theoretical and observational estimates. Assuming the same value of mass  $\nu$  used to obtain our previously quoted result ( $2.5 \times 10^{74} \text{ g cm}^2 \text{ s}^{-1}$ ) and the same redshift ( $z = 3$ ) and distribution of final angular momentum ( $l_f$ ) as adopted by Catelan & Theuns (1996a), we obtain a value for the angular momentum of  $2 \times 10^{74} \text{ g cm}^2 \text{ s}^{-1}$ . This last result is in good agreement with ours and is well in line with previous theoretical estimates (Peebles 1969; Heavens & Peacock 1988) and numerical simulations (Fall 1983). It is obvious that neither the approach used in this paper nor that of Catelan & Theuns (1996a) can predict the very final stages of evolution, when clumps merge and interact nonlinearly and, in addition, dissipative processes may play an important role as well. In any case, the value of the final angular momentum, as obtained from the extrapolation of the linear theory, is typically a factor of  $\simeq 3$  larger than the

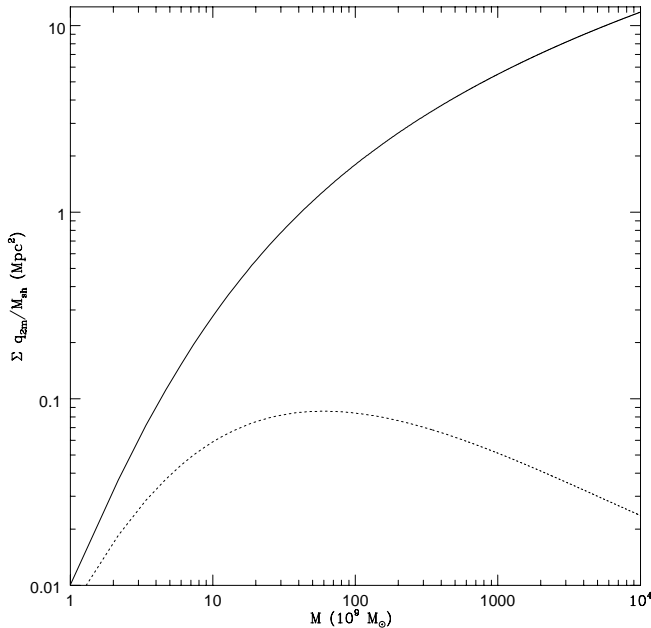


FIG. 1.—Comparison of the mean quadrupole moments due to triaxiality (dotted line) around a  $3\sigma$  peak, smoothed on a galactic scale, with the sum of the rms quadrupole moments due to secondary perturbations (solid line).

final spin of the nonlinear object (Barnes & Efstathiou 1987; Frenk 1987). The effects of this discrepancy can be simply eliminated by reducing the angular momentum by the same factor.

It should be commented that we have used some properties of the random Gaussian fields in order to calculate the torque (e.g., eq. [30]). This could seem a rather strong assumption given that we are concerned with small scales, where the density field is no longer Gaussian. This assumption is justified by the previous remarks, namely, by the fact that our calculation of the final angular momentum is obtained as an extrapolation from linear theory and, as noted above, this approach yields values for the angular momentum that are not too different from those obtained in numerical simulations.

As previously stated, we assume that from  $t_M$  onward the ellipsoid has this constant angular momentum. Following procedure 1 and/or 2 above (§ 2), we can determine the time evolution of the density and the collapse velocity.

#### 4. PARAMETERS, CONSTRAINTS, AND INITIAL CONDITIONS

In order to apply the model introduced in the previous section to the evolution of the collapsing perturbation and solve equations (11)–(14), we need the initial conditions, and moreover, it is necessary to connect these conditions and the time dependence of the shear to properties of the initial density field. To begin with, initially the high-density region that will collapse has  $\delta \ll 1$  and is contained in a spherical region. Following Eisenstein & Loeb (1995), we require that the average mass, density, and quadrupole moments of the ellipsoid match those of the inner spherical region at the initial time. So, defining, as usual, the overdensity of the inner region as

$$\bar{\delta}(R) = \frac{3}{R^3} \int_0^R \delta(y)y^2 dy, \quad (39)$$

the mass of the region is given by

$$M = \frac{4\pi}{3} \rho_b R^3 [1 + \bar{\delta}(R)] = \frac{4\pi}{3} \rho_b R^3 (1 + \nu\sigma). \quad (40)$$

The ellipsoid is chosen to match the previous quantities; it has overdensity  $\bar{\delta}(R)$  and mass  $M = (4\pi/3)\rho_b[1 + \bar{\delta}(R)] \times \alpha_1\alpha_2\alpha_3$ , and by comparison with equation (40), we obtain

$$R^3 = \alpha_1 \alpha_2 \alpha_3. \quad (41)$$

The quadrupole moments, necessary to set  $q_{2m,0}$  in equation (34), are obtained from equation (27). The initial axes of the ellipsoid are fixed as follows: Given a value of  $\delta$  (or  $\nu$ ) and the initial mass,  $M$ , we can calculate the radius  $R$  from equation (40). Equations (41) and (33) make it possible to obtain  $\alpha_1$ ,  $\alpha_2$ , and  $\alpha_3$ . The initial density, for the case  $\nu = 2$ , is  $\delta = 2 \times 10^{-3}$ , and  $M \simeq 2 \times 10^{11} M_\odot$  (since we are concerned with galactic mass scales); the velocity is chosen to be a uniform expansion with the Hubble flow (a pure growing mode).

The equations of the model described in § 2 were integrated using the Bulirsch-Stoer algorithm. We assumed an  $\Omega = 1$  universe and a Hubble constant of  $H_0 = 50 \text{ km s}^{-1} \text{ Mpc}^{-1}$ . The cold dark matter power spectrum that we adopt is  $P(k) = AkT^2(k)$  with the transfer function  $T(k)$

given in BBKS (eq. [G3]),

$$T(k) = \frac{\ln(1 + 2.34q)}{2.34q} [1 + 3.89q + (16.1q)^2 + (5.46q)^3 + (6.71q)^4]^{-1/4}, \quad (42)$$

where  $A$  is a normalization constant and  $q = k\theta^{1/2}/(\Omega_X h^2 \text{ Mpc}^{-1})$ . Here  $\theta = \rho_{\text{cr}}/(1.68\rho_\gamma)$  represents the ratio of the energy density in relativistic particles to that in photons ( $\theta = 1$  corresponds to photons and three flavors of relativistic neutrinos). The spectrum was smoothed on a galactic scale ( $R \simeq 0.5 h^{-1} \text{ Mpc}$ ) and normalized such that  $\sigma(8 h^{-1} \text{ Mpc}) = 1$  at the present epoch ( $\sigma_8$  is the rms value of  $\delta M/M$  in a sphere of  $8 h^{-1} \text{ Mpc}$ ). The mass variance present in equation (38) can be obtained from the spectrum,  $P(k)$ , as

$$\sigma^2(R) = \frac{1}{2\pi^2} \int_0^\infty dk k^2 P(k) W^2(kR), \quad (43)$$

where  $W(kR)$  is a top-hat smoothing function:

$$W(kR) = 3(kR)^{-3}(\sin kR - kR \cos kR). \quad (44)$$

The remaining spectral parameters of equation (38),  $\gamma$  and  $R_*$ , for the chosen spectrum with the above fixed smoothing length, are  $\gamma \simeq 0.6$  and  $R_* = 0.52$ . Regarding the duration of the integration, we followed the suggestions of Eisenstein & Loeb (1995): Since the average overdensity of the innermost external shell is of the same order of magnitude of that of the ellipsoid, the two objects collapse at similar times or, in some cases, the inner external shell collapses before the long axis of the ellipsoid. To avoid this problem, the integration must be stopped at some time before the collapse of the inner tidal shell. This can be accomplished by constraining the initial conditions so that none of the exterior shells has an overdensity greater than 95% of the initial density of the ellipsoid (Eisenstein & Loeb 1995). This last assumption ensures that the external tidal shells do not collapse before the integration ends. As a consequence, the inner region behaves as a density peak. We also imposed the condition  $\bar{\delta}(R_{\text{sphere}}) > \nu\sigma$  with  $\nu > 2$ , implying that the inner spherical regions have high overdensity, and finally, we follow Bond & Myers (1996a, 1996b) in imposing the condition that no axis may collapse below 40% of its maximum length, in order to prevent the dynamics from approaching the singularity at zero length and to simulate virialization of the corresponding axis.

#### 5. RESULTS

The results of the calculations involving the evolution of  $\delta$  are shown in Figures 2–5. In Figure 2, we plot  $\delta = (\rho - \rho_b)/\rho_b$  in the case of a density peak having height  $\nu = \delta/\sigma(R) = 2$ . The solid line represents the solution of equation (14) in the case  $L = \Sigma = 0$ . The dashed and dotted lines, representing the cases ( $L = 0, \Sigma \neq 0$ ) and ( $L \neq 0, \Sigma \neq 0$ ), respectively, were obtained using both procedures 1 and 2 described in § 2. As shown (*dashed line*), the shear produces an enhancement in the growth rate of the density of a mass element. This is the effect first recognized by Hoffman (1986b). The shear term,  $\Sigma^2$ , that appears in the equation for the evolution of the density (eq. [14]) is positive definite, so as long as the fluid is irrotational, the growth rate of the density contrast must be enhanced by it, and thus the effects of the shear are present in both the linear and nonlinear regimes. During the linear phase, the ellipsoid expands with

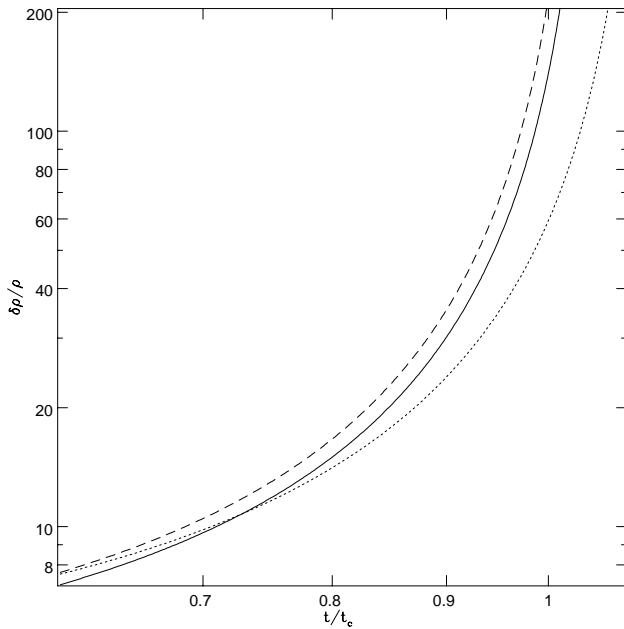


FIG. 2.—Evolution of ellipsoidal density perturbations in an expanding universe as function of redshift for  $\nu = 2$  in the cases  $L = \Sigma = 0$  (solid line),  $L = 0, \Sigma \neq 0$  (dashed line), and  $L \neq 0, \Sigma \neq 0$  (dotted line).

the universe: the tidal field outside the ellipsoid cancels the effects of the gravitational field interior to it. The shear contributes to increase the growth rate of the perturbation. When the effect of the angular momentum can no longer be neglected, we see that the situation changes (dotted line). Initially the shear term dominates, but in a short time the angular momentum begins to influence the growth of the perturbation, counterbalancing the effect of the shear term,  $\Sigma^2$ , and producing a slowing of the growth. As a final result the growth of the density perturbation becomes slower than in the  $L = \Sigma = 0$  case. The density contrast at virialization,  $\delta_v \simeq 60$ , is reduced with respect to the expected value,  $\delta_v \simeq 178$ . The value obtained is intermediate between that obtained by Peebles (1990) for the half-mass radius,  $\delta_v \simeq 30$ , and that obtained with the modified spherical collapse model of Engineer, Kanekar, & Padmanabhan (2000),  $\delta_v \simeq 80$ . We note that in this last paper, the authors showed that to take account of the effects due to the asphericity of a system, one must include in the density evolution equations typical of the spherical collapse model an additive term,  $(1 + \delta)(\Sigma^2 - 2\Omega^2)$ , depending on the shear and angular momentum of the system, similarly to the Nariai & Fujimoto (1972) model.

The preceding result can be interpreted as follows: When the overdensity of the ellipsoid become considerable and  $\delta$  attains amplitudes of order unity, the ellipsoid will begin to recollapse in at least one direction. As shown by Peebles (1980), if we consider the collapse of a sphere of equivalent mass, when this reaches the turnaround epoch one of the axes of the ellipsoid turns shorter and collapses, forming a pancake in which the baryons shock and the dark matter goes through violent relaxation. In the process, the ellipsoid develops nonradial motion. The angular momentum  $L$  present in equations (11)–(14) becomes nonnegligible and produces the slowing of the density growth shown in the figure.

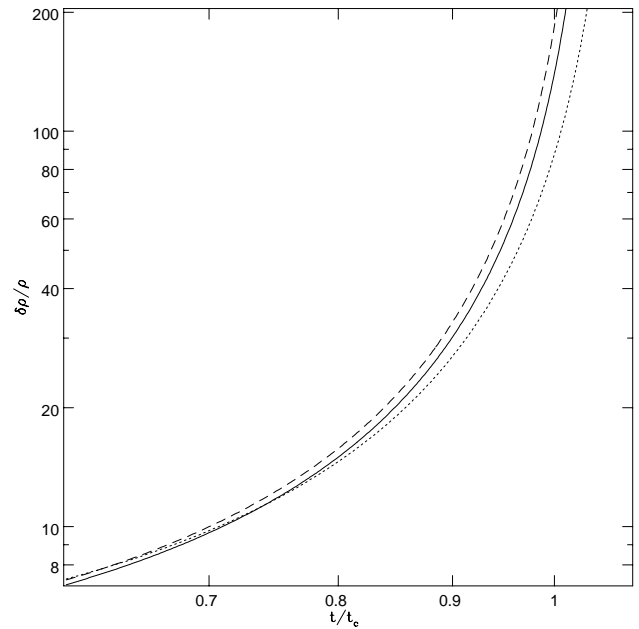


FIG. 3.—Same as Fig. 2, but for  $\nu = 2.5$

In Figure 3, we show the same calculation as in Figure 2, but now we have increased the value of the peak height to  $\nu = 2.5$ . As in the previous case, the shear term produces an enhancement of the density growth rate (dashed line), but this time the effect is smaller with respect to that shown in Figure 2. This is due to the fact that the shear magnitude decreases with increasing peak height (see also Hoffman 1986b, Table 1). As in Figure 2, the angular momentum acts in a sense opposite to that of shear, but this time its effect is reduced (dotted line) with respect to the  $\nu = 2$  case because of the well-known  $L$ - $\nu$  anticorrelation effect (Hoffman 1986a). The trend is confirmed by Figure 4, representing the same calculations as in Figures 2–3 but now for  $\nu = 3$ .

In summary, both  $L$  and  $\Sigma$  exhibit reduced rates of growth with increasing  $\nu$ : rare density peaks are in general

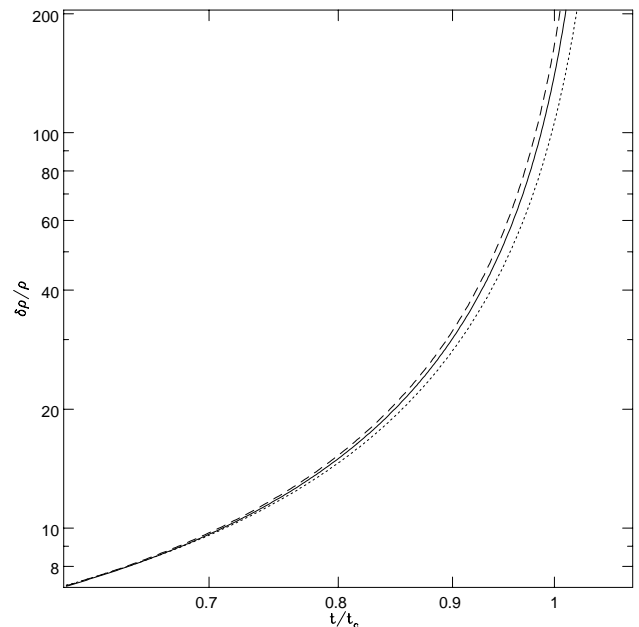


FIG. 4.—Same as Fig. 2, but for  $\nu = 3$

characterized by low shear, and thus the evolution of the perturbation tends to follow the results of the spherical model when  $\nu$  increases, and, as expected, the collapse will also be nearly spherical (Bernardeau 1994).

In order to study the effects of angular momentum and shear on the collapse velocity, we calculate the collapse velocity at the epoch of pancaking numerically, solving the equations of motion for the principal axes of the ellipsoid. Using the notation of Barrow & Silk (1981), we indicate with  $x_0 X(t)$  and  $z_0 Z(t)$  the principal axes ( $x_0$  and  $z_0$  are the initial values). We solve equations (11)–(13) to calculate the collapse velocity down the shortest axis at the epoch of pancaking in the case of an oblate spheroid ( $\alpha_1 = \alpha_2 > \alpha_3$ ). This calculation is similar to that of Barrow & Silk (1981), with the difference that our approach is numerical. Then the collapse velocity at pancaking is

$$v_{z_p} = -z_0 \dot{Z}_p(t) \quad (45)$$

(from here on the subscript  $p$  indicates that the quantity is evaluated at the time of pancaking). The initial conditions are set similarly to those in § 4 and the equations are solved for several values of  $x_0$ , while  $z_0 = 1$ . In Figure 5, we plot  $v_{z_p}/(\dot{a}_p r_p/a_p)$ , where  $r_p = r_0 X_p$  is the pancake radius (see Barrow & Silk 1981), as a function of the ratio of the initial values of the axes,  $x_0/z_0$ . The solid line represents the collapse velocity for an oblate spheroid ( $\alpha_1 = \alpha_2 > \alpha_3$ ) for the case in which  $L \neq 0$ ,  $\Sigma \neq 0$ , and  $\nu = 3$ . The dotted and dashed lines plot the results of the same calculation but for  $\nu = 2.5$  and  $\nu = 2$ , respectively. The figure shows two trends:

1. The collapse velocity is reduced with increasing initial flattening (increasing value of  $x_0$ ). For example, for  $z_0/x_0 = 0.44$  the collapse velocity is reduced to the Hubble velocity in the plane of the pancake ( $H_p r_p$ ), while in the case of the

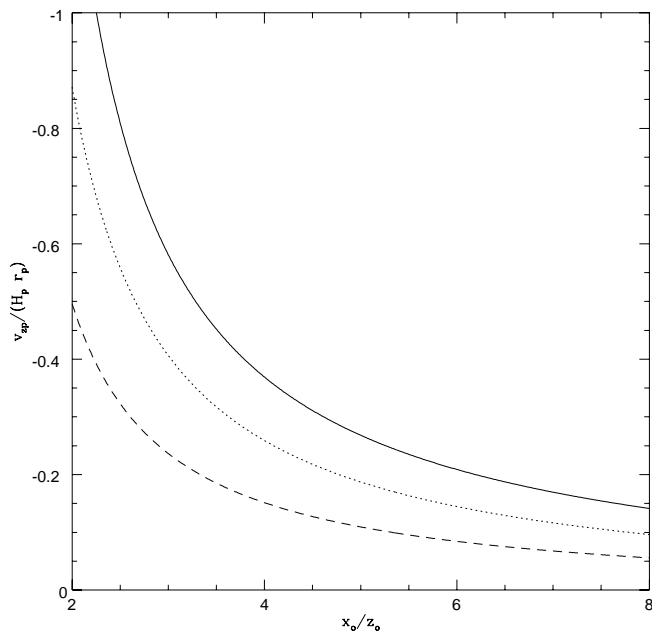


FIG. 5.—Collapse velocity for an oblate spheroid ( $\alpha_1 = \alpha_2 > \alpha_3$ ) down the  $z$ -axis at the epoch of pancaking. Here  $x_0$  and  $z_0$  are the initial values of the longest ( $x$ ) and the shortest ( $z$ ) axis;  $H_p$  and  $r_p$  are respectively the Hubble constant and the pancake radius at the pancaking epoch. The solid line represents the collapse velocity for the case  $L \neq 0$ ,  $\Sigma \neq 0$ , and  $\nu = 3$ . The dotted and dashed lines show the same calculation but for  $\nu = 2.5$  and  $\nu = 2$ , respectively.

more extreme flattening  $z_0/x_0 = 0.125$ , the collapse velocity is reduced by a factor of  $\simeq 6$  with respect the previous value.

2. The collapse velocity is reduced with increasing angular momentum acquired by the protostructure. As shown, the collapse velocity is progressively reduced when we go from  $\nu = 3$  peaks down to  $\nu = 2$ .

In other words, the slowing of the rate of growth of the density contrast produces a lowering of the peculiar velocity, in qualitative and quantitative agreement with Barrow & Silk (1981) and Szalay & Silk (1983).

The result obtained helps to clarify the controversy related to the previrialization conjecture. According to this paper, it is surely true that taking account only of the shear,  $\Sigma$ , produces a shortening of the collapse time of non-spherical perturbations, in agreement with Hoffman (1986b) and Bertschinger & Jain's collapse theorem. The question is that in a real collapse other effects have an important role, namely, external tides and the effects of small-scale substructure. The results of both Hoffman (1986b) and Bertschinger & Jain (1994) are valid for a fluid element, which has no substructure by definition, while a small-scale substructure produces a slowing down of the collapse at least in two ways:

- a) Encounters between infalling clumps and substructure internal to the perturbation (Antonuccio-Delogu & Colafrancesco 1994; Del Popolo & Gambera 1997, 1999); and
- b) Tidal interaction of the main protostructure with substructure external to the perturbation (Peebles 1990; Del Popolo & Gambera 1998).

Moreover, it should be pointed out that as more small-scale power is present, the collapse of a perturbation may be slowed in a way that could inhibit the effect of shear. Differently from Bertschinger & Jain (1994), our model takes into account the angular momentum of the system and, thus, at least the effects produced by point *b* above. Similarly to Bertschinger & Jain (1994), our model fails to take into account the substructure internal to the system. This is a natural limitation of the homogeneous ellipsoid model: a homogeneous ellipsoid cannot represent the substructure of the object. We, recall however, that the same shortcoming was present in Peebles (1990); in that paper, the substructure was suppressed because of the adoption of a homogeneous Poisson distribution of particles within the protocluster. This limitation has the consequence of underestimating the effect of previrialization and, in particular, the value of the overdensity at virialization,  $\delta_v$  (Peebles 1990). In other words, the effects of the slowdown of the collapse obtained in this paper (similarly to that of Peebles 1990) are surely smaller than what we would find if we used a system with internal substructure, as in point *a* above.

Before concluding, we wish to spend a few words on the impact of the results of this paper on our view of structure formation. The reduction in the growth rate of overdensity and collapse velocity has several consequences for structure formation. To begin with, a first consequence is a change of the mass function, the two-point correlation function, and the mass that accretes on density peaks. In fact, as has been remarked several times, the angular momentum acquired by a shell centered on a peak in the cold dark matter density distribution is anticorrelated with density: high-density peaks acquire less angular momentum than do low-density peaks (Hoffman 1986a; R88). A greater amount of angular

momentum acquired by low-density peaks (with respect to the high-density ones) implies that these peaks can more easily resist gravitational collapse, and consequently it is more difficult for them to form structure. This results in a tendency for less dense regions to accrete less mass, with respect to a classical spherical model, inducing a *biasing* of overdense regions toward higher mass.

As a result, the number of objects with  $\sigma \leq 1$  (i.e., high mass) is smaller, since now the collapse is slowed down and the mass function is much below the standard Press-Schechter prediction (Del Popolo & Gambera 1999; Del Popolo et al. 2000; Audit et al. 1997). Even the two-point correlation functions of galaxies and clusters of galaxies are strongly modified as a consequence (see Del Popolo & Gambera 1999; Del Popolo et al. 1999; Peebles 1993).

## 6. CONCLUSIONS

We have examined the evolution of nonspherical inhomogeneities in an Einstein–de Sitter universe by numerically solving the equations of motion for the principal axes and the density of a dust ellipsoid. We took into account the effect of the mass external to the perturbation by calculating

the angular momentum transferred to the developing protostructure by the gravitational interaction of the system with the tidal field of the matter being concentrated in neighboring protostructures.

We showed that for lower values of  $\nu$  ( $\nu = 2$ ), the growth-rate enhancement of the density contrast that is induced by the shear is counterbalanced by the effect of angular momentum acquisition. For  $\nu > 3$ , the effects of angular momentum and shear are reduced, and the evolution of perturbations tends to follow the behavior obtained in the spherical collapse model. These results corroborate the previrialization conjecture because they show that asphericities and tidal torques slow down the collapse of the perturbation after the system detaches from the general expansion.

A. D. P. would like to thank Professor E. Recami and D. Eisenstein for useful comments, and an anonymous referee whose suggestions helped us to considerably improve the quality of this paper. Finally, A. D. P. would like to thank the Boğaziçi University Research Foundation for financial support through project 01B304.

## REFERENCES

- Andriani, E., & Caimmi, R. 1994, *A&A*, 289, 1  
 Antonuccio-Delogu, V., & Colafrancesco, S. 1994, *ApJ*, 427, 72  
 Audit, E., Teyssier, R., & Alimi, J.-M. 1997, *A&A*, 325, 439  
 Bardeen, J. M., Bond, J. R., Kaiser, N., & Szalay, A. S. 1986, *ApJ*, 304, 15 (BBKS)  
 Barnes, J., & Efstathiou, G. 1987, *ApJ*, 319, 575  
 Barrow, J. D., & Silk, J. 1981, *ApJ*, 250, 432  
 Bernardeau, F. 1994, *ApJ*, 427, 51  
 Bertschinger, E., & Jain, B. 1994, *ApJ*, 431, 486  
 Bond, J. R., & Myers, S. T. 1996a, *ApJS*, 103, 1  
 ———. 1996b, *ApJS*, 103, 41  
 Catelan, P., & Theuns, T. 1996a, *MNRAS*, 282, 436  
 ———. 1996b, *MNRAS*, 282, 455  
 Chernin, A. D. 1970, *Pisma Zh. Eksp. Teor. Fiz.*, 11, 317 (English transl. *Soviet Phys.-JETP Lett.*, 11, 210)  
 Davis, M., & Peebles, P. J. E. 1977, *ApJS*, 34, 425  
 Del Popolo, A., & Gambera, M. 1997, *A&A*, 321, 691  
 ———. 1998, *A&A*, 337, 96  
 ———. 1999, *A&A*, 344, 17  
 Del Popolo, A., Gambera, M., Recami, E., & Spedicato, E. 2000, *A&A*, 353, 427  
 Del Popolo, A., Takahashi, Y., Kiuchi, H., & Gambera, M. 1999, *A&A*, 348, 667  
 Doroshkevich, A. G. 1970, *Astrofizika*, 6, 581 (English transl. *Astrophysics*, 6, 320)  
 Eisenstein, D. J., & Loeb, A. 1995, *ApJ*, 439, 520  
 Engineer, S., Kanekar, N., & Padmanabhan, T. 2000, *MNRAS*, 314, 279  
 Evrard, A. E., & Crone, M. M. 1992, *ApJ*, 394, L1  
 Fall, S. M. 1983, in *IAU Symp. 100, Internal Kinematics and Dynamics of Galaxies*, ed. E. Athanassoula (Dordrecht: Reidel), 391  
 Frenk, C. S. 1987, in *Nearly Normal Galaxies*, ed. S. M. Faber (New York: Springer), 421  
 Heavens, A., & Peacock, J. 1988, *MNRAS*, 232, 339  
 Hoffman, Y. 1986a, *ApJ*, 301, 65  
 ———. 1986b, *ApJ*, 308, 493  
 ———. 1989, *ApJ*, 340, 69  
 Hoyle, F. 1951, in *Problems of Cosmical Aerodynamics*, ed. J. M. Burgers & H. C. van de Hulst (Dayton: Cent. Air Doc. Off.), 195  
 Łokas, E. L., Juszkiewicz, R., Bouchet, F. R., & Hivon, E. 1996, *ApJ*, 467, 1  
 Monaco, P. 1995, *ApJ*, 447, 23  
 Nariai, H., & Fujimoto, M. 1972, *Prog. Theor. Phys.*, 47, 105  
 Peebles, P. J. E. 1969, *ApJ*, 155, 393  
 ———. 1980, *The Large-Scale Structure of the Universe* (Princeton: Princeton Univ. Press)  
 ———. 1990, *ApJ*, 365, 27  
 ———. 1993, *Principles of Physical Cosmology* (Princeton: Princeton Univ. Press)  
 Peebles, P. J. E., & Groth, E. J. 1976, *A&A*, 53, 131  
 Pichon, C., & Bernardeau, F. 1999, *A&A*, 343, 663  
 Ryden, B. S. 1988, *ApJ*, 329, 589 (R88)  
 Ryden, B. S., & Gunn, J. E. 1987, *ApJ*, 318, 15  
 Sasaki, M., & Kasai, M. 1998, *Prog. Theor. Phys.*, 99, 585  
 Szalay, A. S., & Silk, J. 1983, *ApJ*, 264, L31  
 Villumsen, J. V., & Davis, M. 1986, *ApJ*, 308, 499  
 White, S. D. M. 1984, *ApJ*, 286, 38  
 White, S. D. M., & Silk, J. 1979, *ApJ*, 231, 1  
 Zeldovich, Ya. B. 1970, *A&A*, 5, 84  
 Zeldovich, Ya. B., & Novikov, I. D. 1983, *Relativistic Astrophysics*, Vol. 2, *The Structure and Evolution of the Universe* (rev. enlarged ed.; Chicago: Univ. Chicago Press)